Supplement of Earth Syst. Dynam., 16, 1483–1501, 2025
https://doi.org/10.5194/esd-16-1483-2025-supplement

Earth System Dynamics
Open Access
EGU

Supplement of

Simple physics-based adjustments reconcile the results of Eulerian and Lagrangian techniques for moisture tracking in atmospheric rivers

Alfredo Crespo-Otero et al.

Correspondence to: Alfredo Crespo-Otero (alfredocrespo.otero@usc.es)

S1 Supplementary figures for the selected AR cases

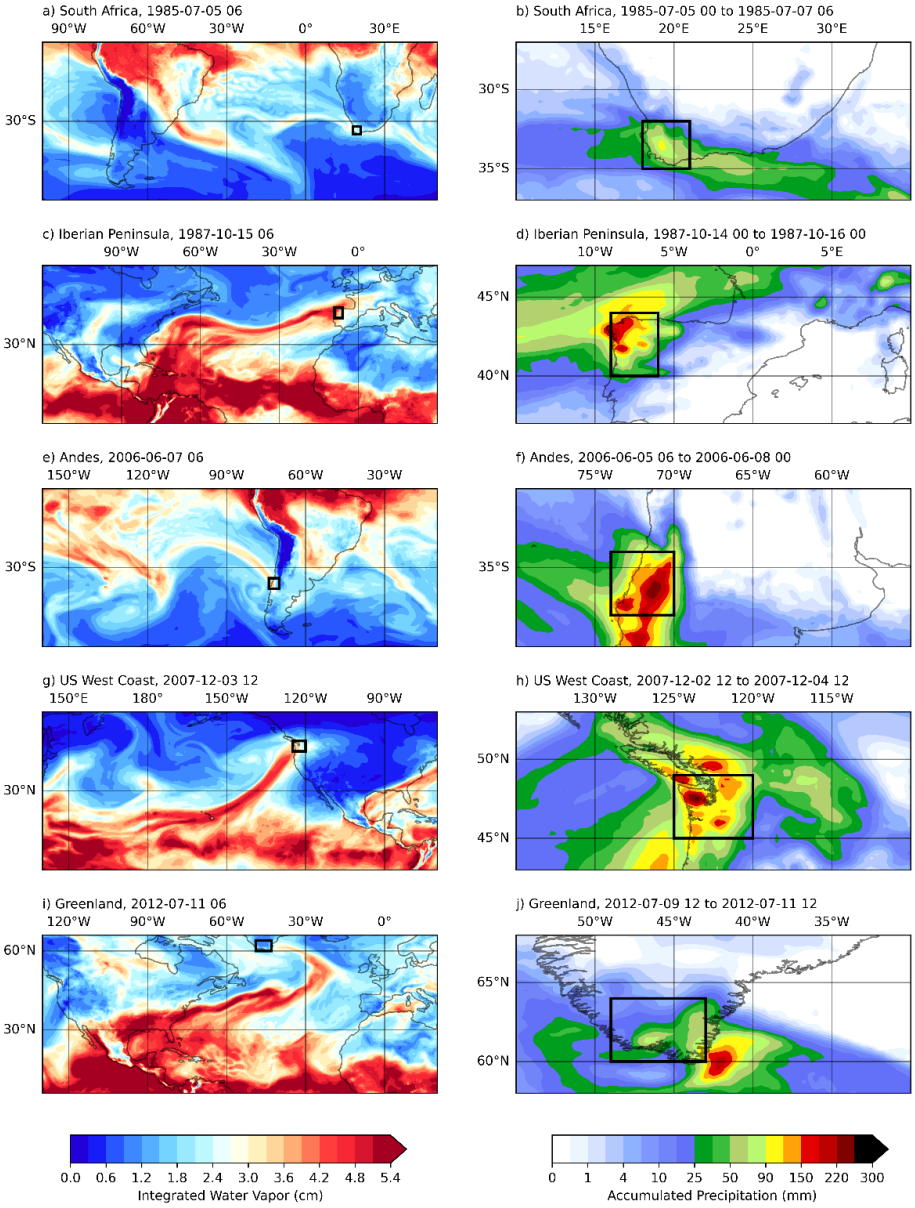

Figure S1: Precipitable water during the selected AR-related precipitation events (left) and accumulated precipitation during the entire episodes (right), from the ERA5 reanalysis. The black boxes are the regions in which precipitation is tracked.

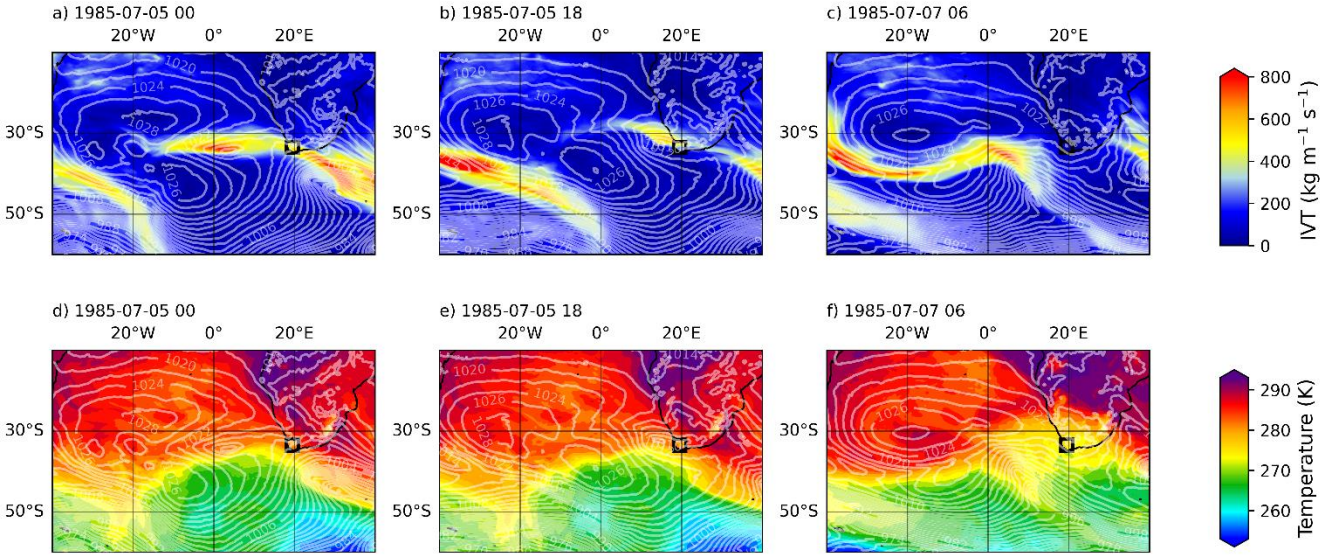

Figure S2: Integrated Vapor Transport (IVT; top) and 850 hPa temperature (bottom), together with the sea level pressure, for the South Africa rainfall event. The represented fields are obtained from the WRF simulation.

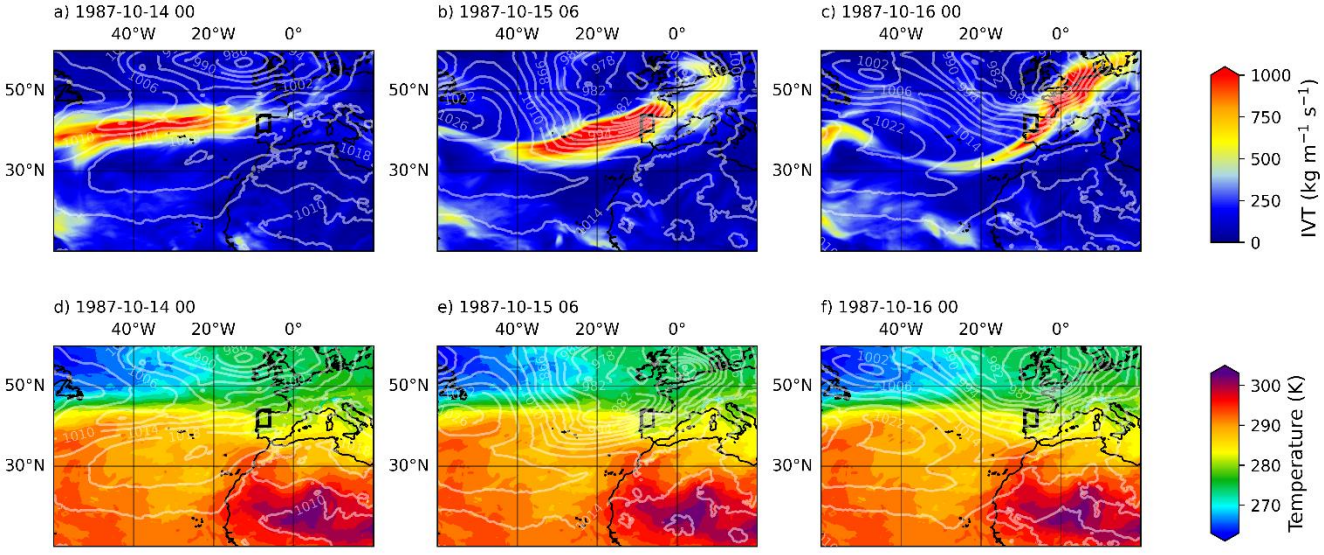

Figure S3: Integrated Vapor Transport (IVT; top) and 850 hPa temperature (bottom), together with the sea level pressure, for the Iberian Peninsula rainfall event. The represented fields are obtained from the WRF simulation.

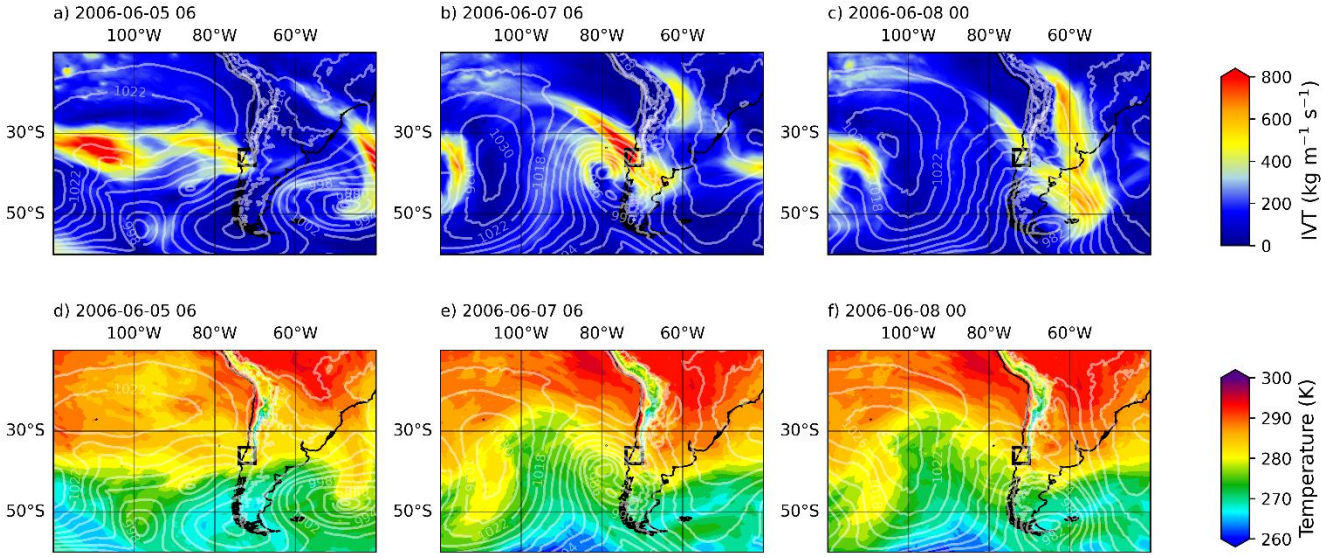

Figure S4: Integrated Vapor Transport (IVT; top) and 850 hPa temperature (bottom), together with the sea level pressure, for the Andes rainfall event. The represented fields are obtained from the WRF simulation.

15

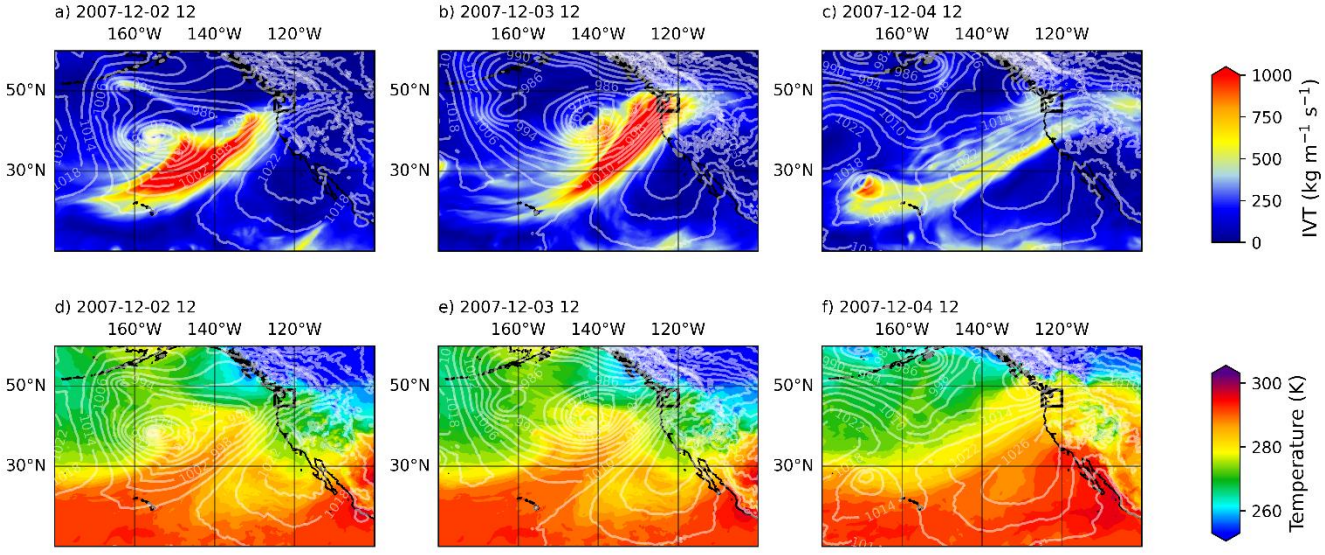

Figure S5: Integrated Vapor Transport (IVT; top) and 850 hPa temperature (bottom), together with the sea level pressure, for the US West Coast rainfall event. The represented fields are obtained from the WRF simulation.

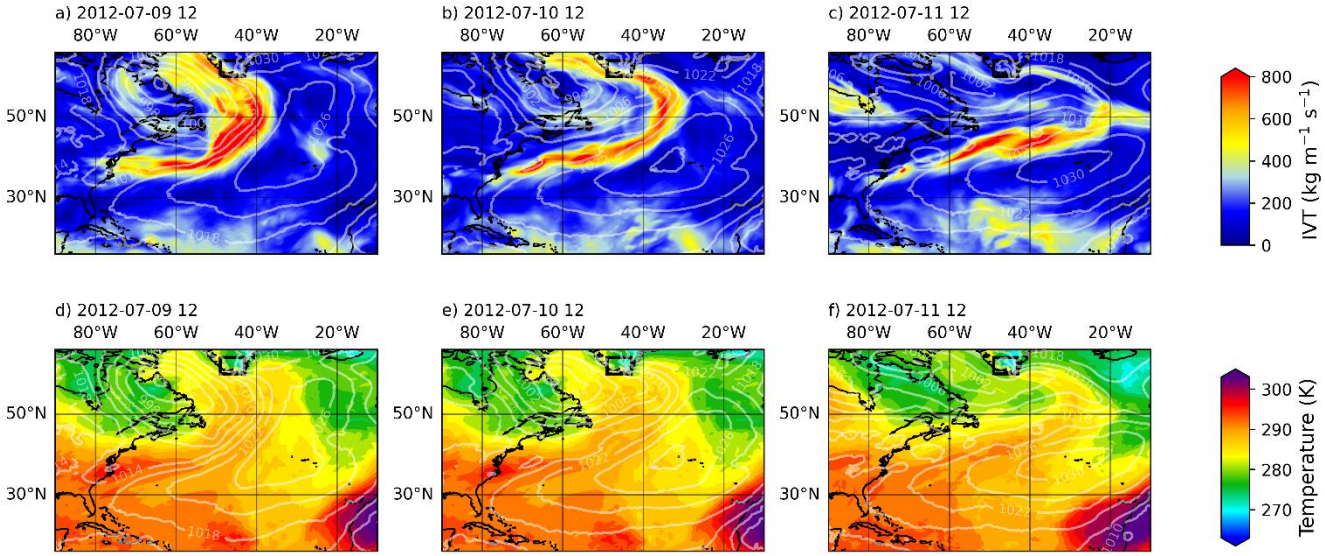

20 Figure S6: Integrated Vapor Transport (IVT; top) and 850 hPa temperature (bottom), together with the sea level pressure, for the Greenland rainfall event. The represented fields are obtained from the WRF simulation.

S2 Supplementary methods

We provide here a detailed description of the configurations of the WRF-WVTs, FLEXPART-WRF and FLEXPART simulations. Although in the methods section of the main text the most relevant aspects were already covered, we include here additional details that may be important to reproduce the results of this study.

S2.1 WRF-WVTs simulations

In this study we use the WRF model version 4.3.3 with Water Vapor Tracers (WRF-WVTs; Insua-Costa and Miguez-Macho, 2018), with the solely modification of simulating the reanalysis evaporation, which we explained in the main manuscript. Next, we provide some additional details regarding the spatial and temporal discretization, together with the different physical parameterizations used in our simulations.

- As already indicated, all simulations start 30 days before the beginning of the rainfall episode. Boundary conditions are updated every 6 hours, and evaporation data is read hourly. The model time step is set to 60 seconds, and it produces output every 3 hours.
- To create the domains shown in the main manuscript, we used a Mercator projection with true latitude at 45° N and 45° S for Ars occurring in the Northern and Southern hemisphere, respectively. The 20 km × 20 km grid consists of 1216 grid points in the W-E direction and 362 grid points in the S-N direction.
- The physical parameterizations are those where the water vapor tracers are implemented. This involves selecting the Yonsei University Scheme as the boundary layer parameterization; the WRF Single-Moment 6-class as the microphysics parameterization, and the Kain–Fritsch scheme for the convective parameterization. Regarding the radiation schemes, the Rapid Radiative Transfer Model and Dudhia schemes are used for long and short wave radiation, respectively. Finally, the Noah land surface model and the Revised MM5 Monin-Obukhov scheme are used as surface-layer and land-surface options.

S2.2 FLEXPART-ERA5 and FLEXPART-WRF simulations

Regarding the Lagrangian models, we use the FLEXPART-WRF model version 3.1 (Brioude et al., 2013), and the FLEXPART (from now on, FLEXPART-ERA5) model version 10.4 (Pisso et al., 2019). In both models a modification is introduced to allow the release of parcels in a box using the domain-filling option (that is, the vertical distribution of parcels follow the density profile), for then computing the trajectories as usual in a global domain. As before, some relevant details are given below.

- As with WRF-WVTs, all simulations cover the 30 days prior to the rainfall episode, together with the latter. In the case of FLEXPART-WRF, input fields are read from the WRF output every 3 hours, while FLEXPART-ERA5 reads ERA5 input data hourly. Regarding the time step, both FLEXPART-ERA5 and FLEXPART-WRF adapt the integration time step to the Lagrangian timescales τ_{Li}, where i is one of the three wind components. In our case, the

time step must be 10 times smaller than τ_{Li} (CTL=10), and for vertical motions it is decreased by a factor 10 (IFINE=10). Both models produce hourly output.

- Regarding the spatial resolution of the input data, FLEXPART-WRF uses WRF input data, so it ingests fields at 20 km horizontal resolution and at 38 pressure levels. In the case of FLEXPART-ERA5, the horizontal resolution of ERA5 data is degraded to 0.5° for storage purposes, and the model ingests fields in the lowest 70 IFS model levels.
- Finally, both FLEXPART-ERA5 and FLEXPART-WRF diagnose turbulence and convection in an equivalent way. For turbulence, a Langevin equation is solved for each wind component, and Gaussian turbulence is assumed. In the case of convection, the Emmanuel scheme is used.

S3 Additional information about the Lagrangian moisture source diagnostics

In this section, we delve into further details mentioned in the main text regarding the Lagrangian moisture source diagnostics used in this study, namely the Sodemann et al., (2008) and the Dirmeyer and Brubaker, (1999) methodologies (hereafter, SOD08 and DB99). First, we give an in-depth explanation of both methodologies and their similarities, with a particular emphasis on the discounting procedures. Then we present a more technical exposition of the physics-based modification applied to the DB99 moisture source diagnostic.

S3.1 More details on the SOD08 and DB99 methodologies

First, recall that the SOD08 diagnostic tool starts by computing the moisture differences $\Delta q_{\mathrm{parcel},t}$,

$$\Delta q_{\mathrm{parcel},t} = q_{\mathrm{parcel},t} - q_{\mathrm{parcel},t-1} = f_{\mathrm{parcel},t} q_{\mathrm{parcel},t}, \tag{S1}$$

where we are using the notation $q_{\mathrm{parcel},t} = q\left(\vec{r}_{\mathrm{parcel},t}, t\right)$ and the relative moisture increments $f_{\mathrm{parcel},t}$ have been introduced. Observe that the absolute value of these quantities is always equal or smaller than 1 by definition. Next, for each parcel, the absolute and fractional contributions of each time step where an uptake occurs (that is, an increment in moisture takes place) are initialized as $\Delta q^0_{\mathrm{parcel},t} = \Delta q_{\mathrm{parcel},t}$, $f^0_{\mathrm{parcel},t} = f_{\mathrm{parcel},t}$. Now we will explain how the discounting procedure affects these two quantities. Let us assume that it has been applied until time *t'*, so that we have the absolute and fractional contributions, $\Delta q^{t'-1}_{\mathrm{parcel},t}$ and $f^{t'-1}_{\mathrm{parcel},t}$ for a certain parcel.

- On the one hand, suppose that at *t'* there is a moisture increase, so that $\Delta \mathrm{q}_{\mathrm{parcel},t'} > 0$. In this case the absolute contributions remain the same, $\Delta q^{t'}_{\mathrm{parcel},t} = \Delta q^{t'-1}_{\mathrm{parcel},t}$ for $t < t'$, whereas the fractional ones must be updated:

$$f^{t'}_{\mathrm{parcel},t} = \frac{\Delta q^{t'-1}_{\mathrm{parcel},t}}{q_{\mathrm{parcel},t'}} = \frac{\Delta q^{t'-1}_{\mathrm{parcel},t}}{\frac{q_{\mathrm{parcel},t'-1}}{1-f_{\mathrm{parcel},t'}}} = f^{t'-1}_{\mathrm{parcel},t}\left(1 - f_{\mathrm{parcel},t'}\right) = f^{t'-1}_{\mathrm{parcel},t} \frac{q_{\mathrm{parcel},t'-1}}{q_{\mathrm{parcel},t'}}, \tag{S2}$$

  where Eq. (S1) has been used to write $q_{\mathrm{parcel},t'}$ as $\frac{q_{\mathrm{parcel},t'-1}}{1-f_{\mathrm{parcel},t'}}$. Observe that $f^{t'}_{\mathrm{parcel},t} < f^{t'-1}_{\mathrm{parcel},t}$.

- On the other hand, in the case $\Delta q_{\mathrm{parcel},t'} < 0$ the absolute contributions do need an update. Again, using the relation between $q_{\mathrm{parcel},t'}$ and $f_{\mathrm{parcel},t'}$ we can write:

$$\Delta q^{t'}_{\mathrm{parcel},t} = \Delta q^{t'-1}_{\mathrm{parcel},t} + \Delta q_{\mathrm{parcel},t'} \frac{\Delta q^{t'-1}_{\mathrm{parcel},t}}{q_{\mathrm{parcel},t'-1}} = \Delta q^{t'-1}_{\mathrm{parcel},t} \left(1 - \frac{\left|\Delta q_{\mathrm{parcel},t'}\right|}{q_{\mathrm{parcel},t'-1}}\right), \tag{S3}$$

  so that $\Delta q^{t'}_{\mathrm{parcel},t} < \Delta q^{t'-1}_{\mathrm{parcel},t}$. In terms of $f_{\mathrm{parcel},t'}$:

$$\Delta q^{t'}_{\mathrm{parcel},t} = \Delta q^{t'-1}_{\mathrm{parcel},t} \left(1 + \frac{\Delta q_{\mathrm{parcel},t'}}{q_{\mathrm{parcel},t'}\left(1-f_{\mathrm{parcel},t'}\right)}\right) = \Delta q^{t'-1}_{\mathrm{parcel},t} \left(1 + \frac{f_{\mathrm{parcel},t'}}{1-f_{\mathrm{parcel},t'}}\right) = \Delta q^{t'-1}_{\mathrm{parcel},t} \frac{1}{1-f_{\mathrm{parcel},t'}}. \tag{S4}$$

  Thus, the fractional contributions $f^{t'}_{\mathrm{parcel},t}$ remain the same, since the factor $\left(1 - f_{\mathrm{parcel},t}\right)^{-1}$ cancels out.

Up to that point we have illustrated how to use both the fractional and the absolute contributions in SOD08 to apply the discounting procedure. In the first case an update is needed at uptake locations, whereas in the second one, the update must

occur at loss sites. The procedure continues until reaching the most recent time step. Then the final aggregation over parcels to obtain the moisture sources is done as explained in the methods section of the main manuscript.

On the other hand, in the case of the DB99 methodology we will reason with its forward version, implemented in the UTrack-atmospheric-moisture model (Tuinenburg and Staal, 2020). Within this framework, the water content in mm of each parcel $W_{\text{parcel},t}$ is computed using the following equation:

$$W_{\text{parcel},t} = W_{\text{parcel},t-1} + \left(E_{x,y,t} - P_{x,y,t}\right)\frac{W_{\text{parcel},t-1}}{PW_{x,y,t}} = W_{\text{parcel},t-1}\left(1 + \frac{E_{x,y,t}-P_{x,y,t}}{PW_{x,y,t}}\right), \tag{S5}$$

where $E_{x,y,t}$, $P_{x,y,t}$ and $PW_{x,y,t}$ are the evapotranspiration, precipitation and precipitable water reanalysis at location (x,y) and time t, being x and y given by the parcel position. When the model is run forward in time, a certain source is selected, and for every parcel a fraction of its water content coming from that source at every time t is computed, $E^{\text{source}}_{\text{parcel},t}$. Thus, $E^{\text{source}}_{\text{parcel},t}$ $W_{\text{parcel},t}$ is the amount of water in the parcel proceeding from the same source at time t. If we denote this quantity by $W^{\text{source}}_{\text{parcel},t}$, the update formulas for both $W^{\text{source}}_{\text{parcel},t}$ and $E^{\text{source}}_{\text{parcel},t}$ are

$$W^{\text{source}}_{\text{parcel},t} = W^{\text{source}}_{\text{parcel},t-1} - P_{x,y,t}\frac{W^{\text{source}}_{\text{parcel},t-1}}{PW_{x,y,t}} = W^{\text{source}}_{\text{parcel},t-1}\left(1 - \frac{P_{x,y,t}}{PW_{x,y,t}}\right), \tag{S6}$$

$$E^{\text{source}}_{\text{parcel},t} = \frac{W^{\text{source}}_{\text{parcel},t-1}\left(1-\frac{P_{x,y,t}}{PW_{x,y,t}}\right)}{W_{\text{parcel},t-1}\left(1+\frac{E_{x,y,t}-P_{x,y,t}}{PW_{x,y,t}}\right)} = E^{\text{source}}_{\text{parcel},t-1}\frac{PW_{x,y,t}-P_{x,y,t}}{PW_{x,y,t}-P_{x,y,t}+E_{x,y,t}}. \tag{S7}$$

The similarities between Eq. (S2) and (S3), and Eq. (S6) and (S7), are clear. Observe that there is not update in the equation for $W^{\text{source}}_{\text{parcel},t}$ if $P_{x,y,t} = 0$, just as it happens with the absolute contributions in SOD08 when $\Delta q_{\text{parcel},t} > 0$. In that case, the quantity $E^{\text{source}}_{\text{parcel},t}$ is effectively reduced if there is evaporation according to Eq. (S7), as the relative contributions in SOD08, Eq. (S2). On the other hand, if $E_{x,y,t} = 0$ it is clear that $E^{\text{source}}_{\text{parcel},t} = E^{\text{source}}_{\text{parcel},t-1}$, and the same follows for SOD08 when $\Delta q_{\text{parcel},t} < 0$: the relative contributions remain the same. A difference between both methodologies may arise, however, when both $E_{x,y,t}$ and $P_{x,y,t}$ are positive, as SOD08 is not able to separate evaporation from precipitation in the surface freshwater flux E-P.

To summarize, both methodologies are mainly equivalent up to the following identifications.

- The interpolated specific humidity in SOD08 corresponds to the computed water content given by Eq. (5) inDB99. Thus, the positive moisture increments $\Delta q_{\text{parcel},t}$ in the first case correspond to relative increments of magnitude $E_{x,y,t} / PW_{x,y,t}$ in the second one.
- The factor by which moisture content is reduced in SOD08 is given by a relative decrease in specific humidity, $\left|\Delta q_{\text{parcel},t}\right| / q_{\text{parcel},t-1}$, whereas in DB99 the same factor is computed as $P_{x,y,t} / PW_{x,y,t}$.

In both cases the parcel is assumed to be over (x,y) at time t.

S3.2 A threshold for parcel height release in the DB99 methodology

After the exposition of our main results, we have argued why including all parcels in the calculation of moisture sources of the DB99 moisture source diagnostic may lead to an underestimation of remote contributions. Specifically, the DB99 methodology weights parcels according to their humidity, so parcels near the surface are given more relevance in the calculation. However, in the type of precipitation event we are considering those parcels rarely contribute to rainfall. In what follows we will try to explain this underestimation from a more technical perspective. We remark that this discussion, together with the proposed modification, concerns only the backwards version ofthe DB99 methodology. In the UTrack-atmospheric-moisture model the same method is also implemented forward in time and, as explained in Tuinenburg and Staal, (2020), the realistic and default configuration is to release parcels from the surface, where evaporation occurs.

To begin with, we will follow the work of Dirmeyer and Brubaker, (1999) to explain in detail how parcels were released in this original study to determine the moisture sources for precipitation. Specifically, let us assume a grid box i where precipitation has occurred. At any level $\sigma = c$, the column precipitable water below that level in kg m^{-2} is

$$PW_c = \frac{p_s}{g}\int_c^1 q(\sigma)d\sigma = \int_{z_c}^{\text{Top atm.}} q(z)\rho(z)dz, \quad \text{(S8)}$$

where the hydrostatic equation has been used to change from sigma-levels to height coordinates. Then parcels are vertically distributed such that the probability of a trajectory starting at level $\sigma \leq c$ is

$$P_c = 1 - \frac{PW_c}{PW_i}, \quad \text{(S9)}$$

where PW_i is the total precipitable water over grid box i. By doing that parcels are released in height following the humidity profile. More precisely, not the specific humidity profile, but $\rho(z)q(z)$, which is proportional to the amount of water at level z. This assumes that every water vapor molecule in the precipitating column has an equal probability of being rained out, that is, each layer of the atmospheric column over grid box i contributes to precipitation according to its water content, so most of the rain comes from the lower levels.

In this context, we remark that $\mathrm{f(z)} = 1/(\mathrm{PWi})\mathrm{q(z)}\rho\mathrm{(z)}$ is a probability density function (PDF) for the release height, and some quantities may be written as averages with respect to this PDF,

$$PW_i = \langle PW_i \rangle,\ P_i = \langle P_i \rangle, \quad \text{(S10)}$$

Where P_i is the rainfall in grid box i. Importantly, the 2-D field of moisture sources for P_i, $MS_i(\lambda,\varphi)$, can be expressed as follows:

$$MS_i(\lambda,\phi) = \frac{P_i}{PW_i}\left(\int_0^{\text{Top atm}} ms_i(\lambda,\phi;z)q(z)\rho(z)\right)dz\ = \langle P_i ms_i(\lambda,\phi;z)\rangle, \quad \text{(S11)}$$

where $ms_i(\lambda,\phi;z)$ is the spatial distribution of sources for moisture at height z over grid box i. Thus, the modification we propose may be expressed in this formalism introducing a function $c(z)$ indicating the contribution of each atmospheric layer over grid box i to precipitation, that is

$$PW_i = \langle PW_i \rangle,\ P_i = \langle c(z) P_i \rangle, MS_i(\lambda, \phi) = \langle P_i\ c(z)\ ms_i(\lambda, \phi; z) \rangle$$

Since we do not know $c(z)$, we propose a piecewise function,

$$c(z) = \begin{cases} 0, & z \leq 2\ km, \\ \frac{1}{PW_{2\ km}}, & z > 2\ km, \end{cases} \quad \text{(S12)}$$

being $PW_{2\ km}$ the column precipitable water above 2 km, which our analysis has shown to enhance the compatibility with WRF-WVTs.

Finally, we remark that in our case we use FLEXPART to generate the trajectories, so that parcels are vertically released following the density profile (using the domain-filling option). In that case the p.d.f is $f(z) = \rho(z)/M_i$, where M_i is the atmospheric mass (in kg m^{-2}) over grid box *i*. In that context the averages in Eq. (S11) must be computed multiplying by $q(z)$, and the rest of the exposition would remain the same.

S4 Supplementary results

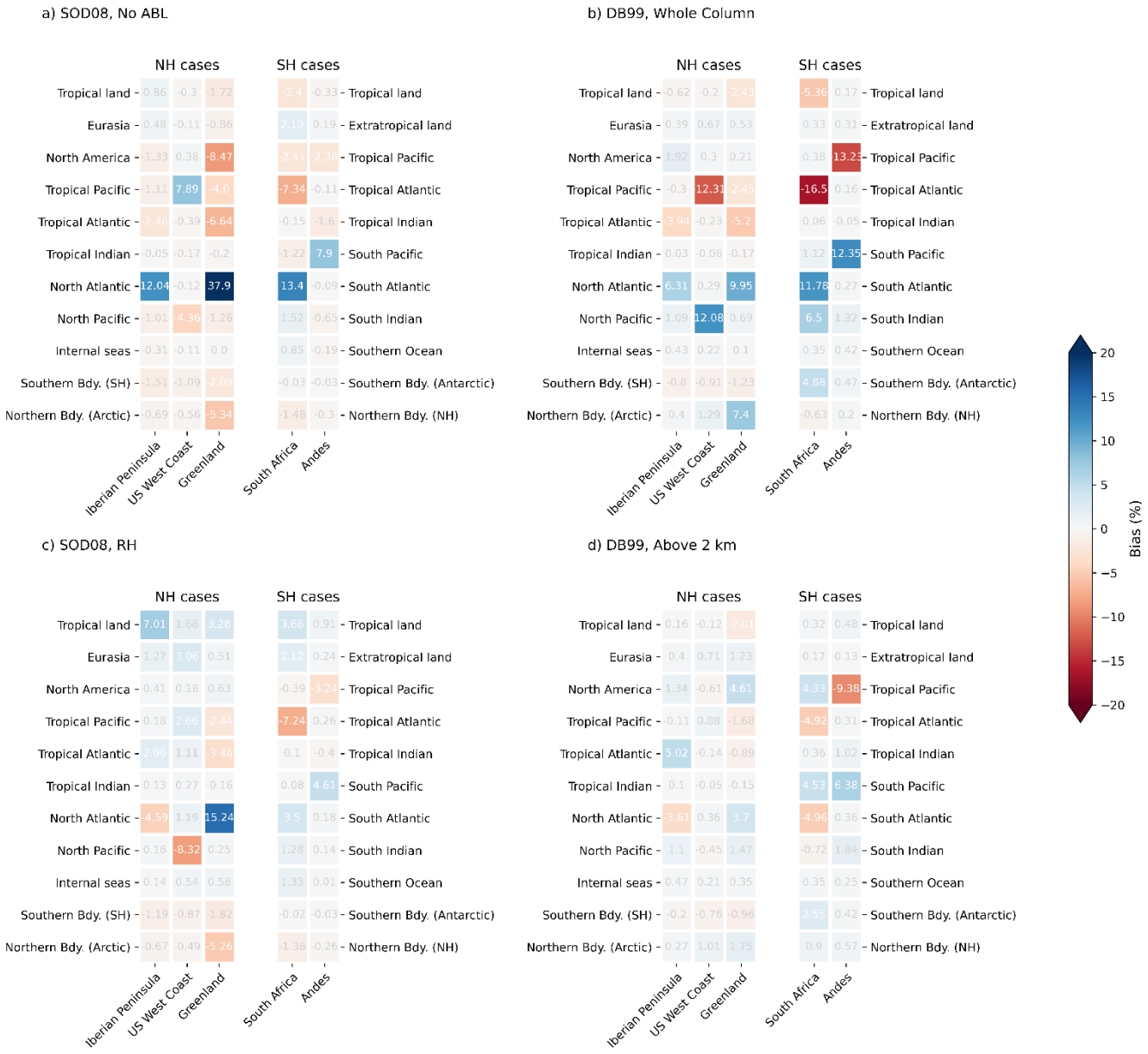

165 Figure S7: Bias in the precipitation fraction (%) obtained using the basic (a and b) and modified (c and d) configurations of the SOD08 (left) and DB99 (right) moisture source diagnostics, for trajectories generated with FLEXPART-WRF. Biases are computed subtracting the "true" outcomes of WRF-WVTs from the corresponding values of SOD08 and DB99.

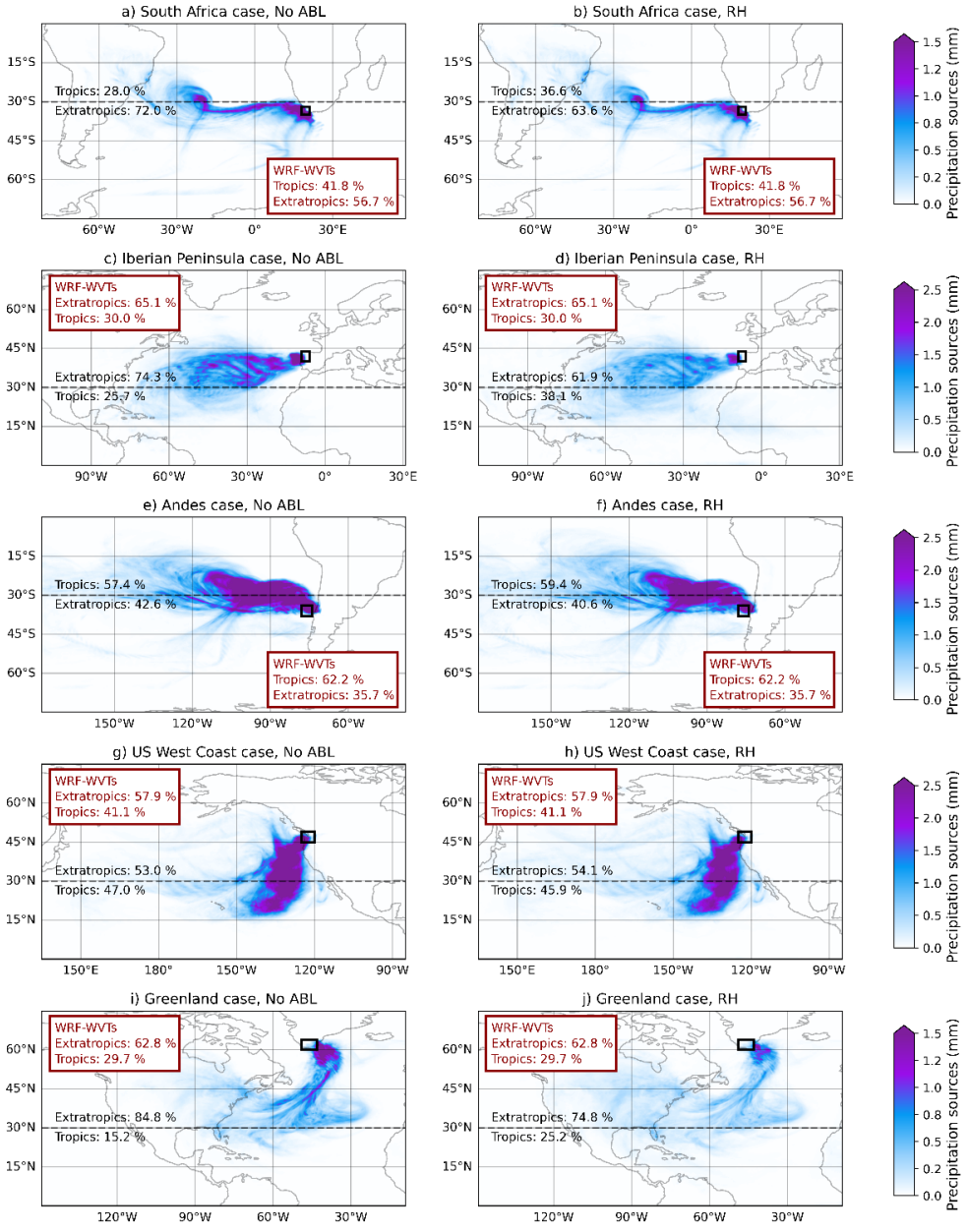

Figure S8: Precipitation sources for the different AR-related rainfall events, computed with the SOD08 diagnostic, for trajectories generated with FLEXPART-WRF. Panels show the results for the most basic configuration, while panels on the right present the results of the "RH" configuration. The fraction of precipitation coming from the tropics and the extratropics is shown in black for each case, and the red box shows these same contributions from WRF-WVTs.

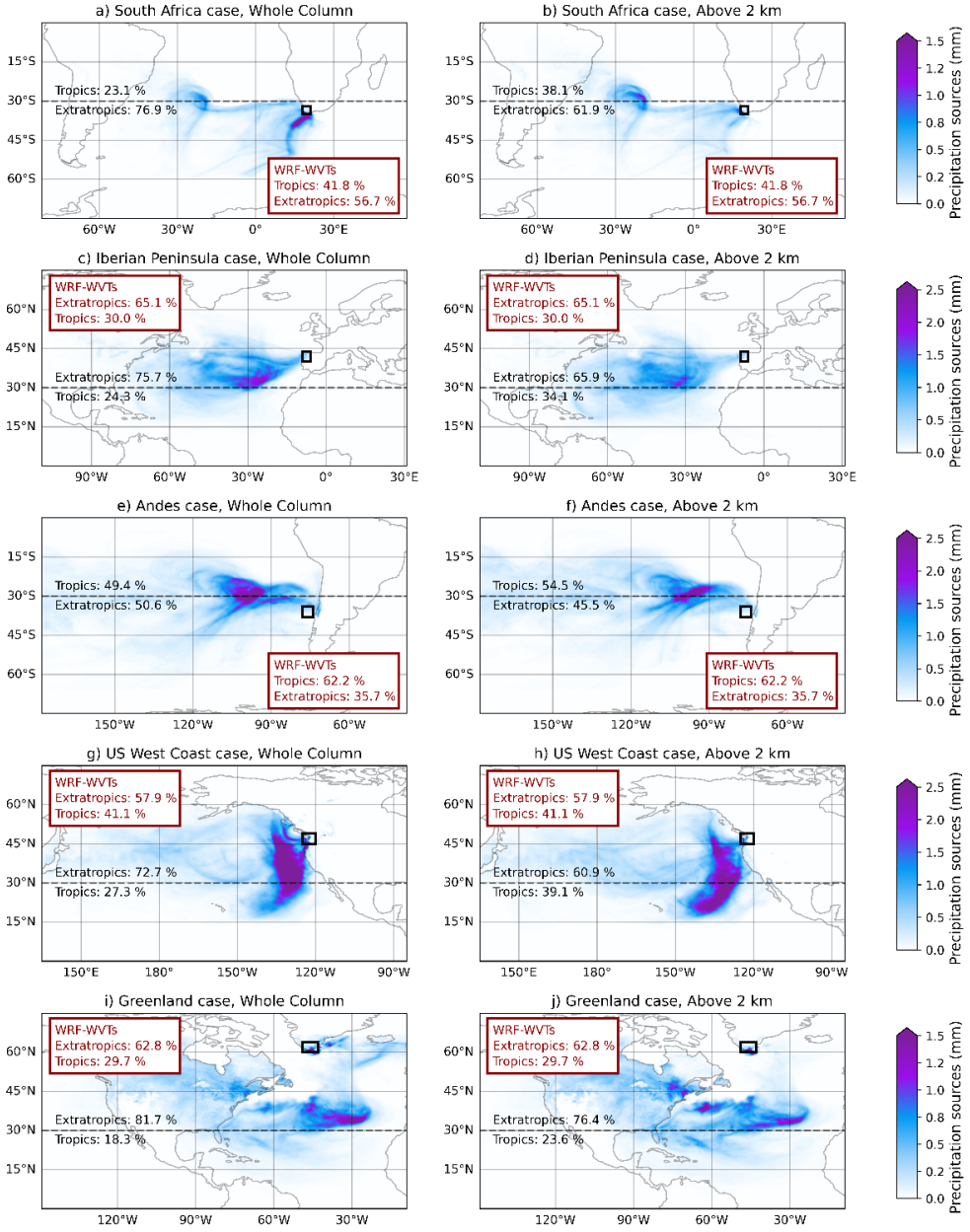

Figure S9: Precipitation sources for the different AR-related rainfall events, computed with the DB99 model, for trajectories generated with FLEXPART-WRF. Panels show the results for the most basic configuration, while in panels on the right parcels below 2 km are not considered. The fraction of precipitation coming from the tropics and the extratropics is shown in black for each case, and the red box shows these same contributions from WRF-WVTs.

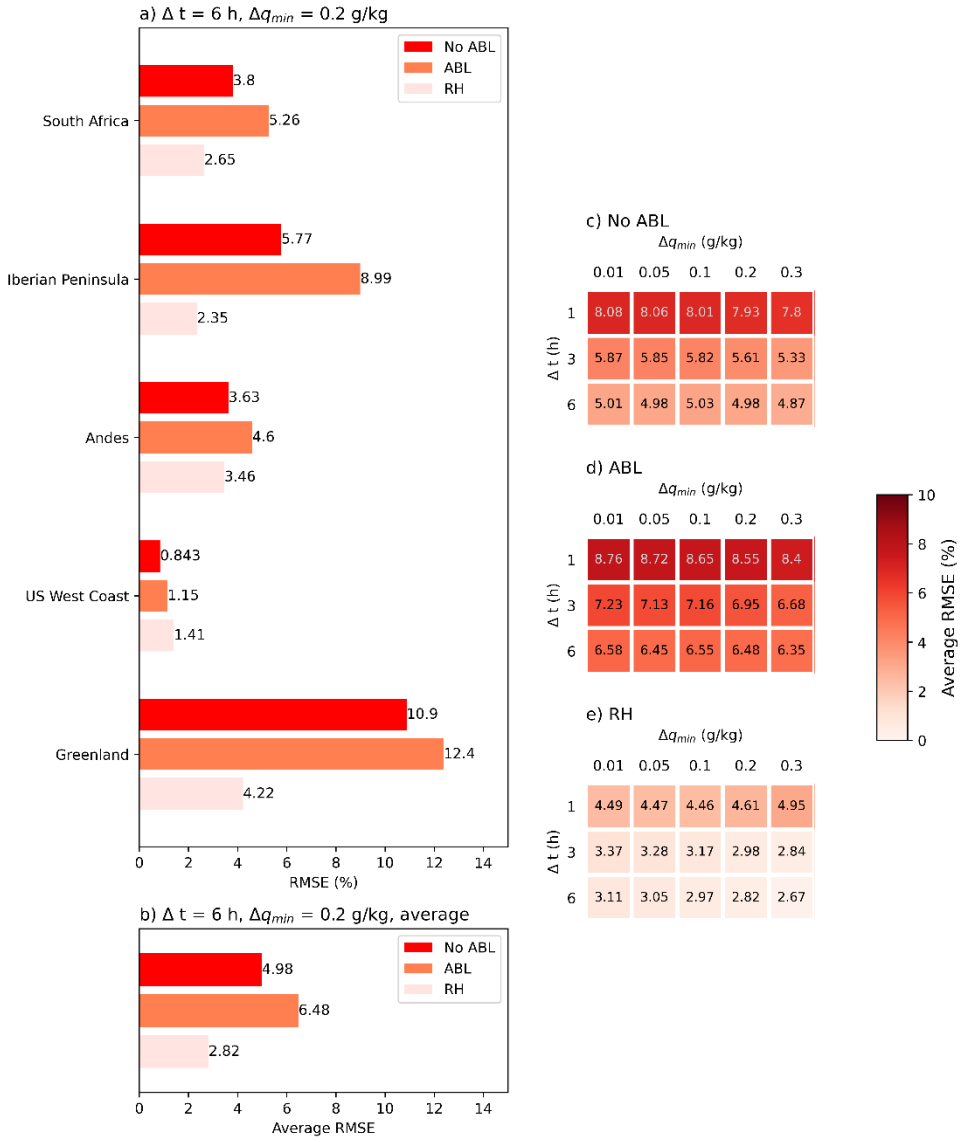

Figure S10: On the left, RMSE for the five AR-related precipitation events (panel a), and average of all of them (panel f), for the standard choice of the specific humidity threshold and time step. The trajectories are computed with FLEXPART-ERA5. On the right, average RMSE for different values of the specific humidity threshold and time step of the SOD08 methodology, in the case of the most basic configuration (No ABL, panel c), neglecting increments above the ABL (ABL, panel d), and discarding decreases below a minimum relative humidity (RH, panel e).

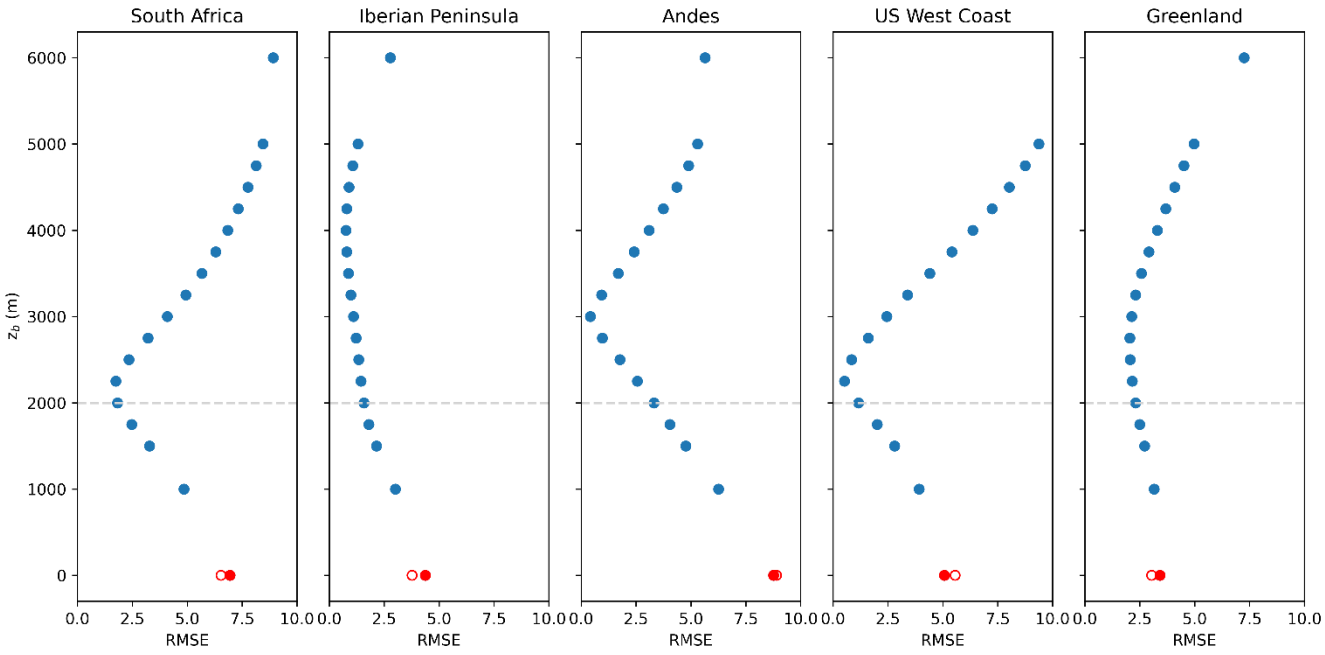

Figure S11: Variation of the RMSE with a threshold height z_b for parcel release in each AR-related rainfall event. True values are from WRF-WVTs, and predicted values are computed with the DB99 methodology, excluding parcels whose initial height is below z_b and relative humidity below 80 %. In red, the RMSE for the original configuration including all parcels (empty dot) and applying the relative humidity filter (filled dot). The dashed line indicates the 2 km threshold selected. The trajectories are computed with FLEXPART-ERA5.

210

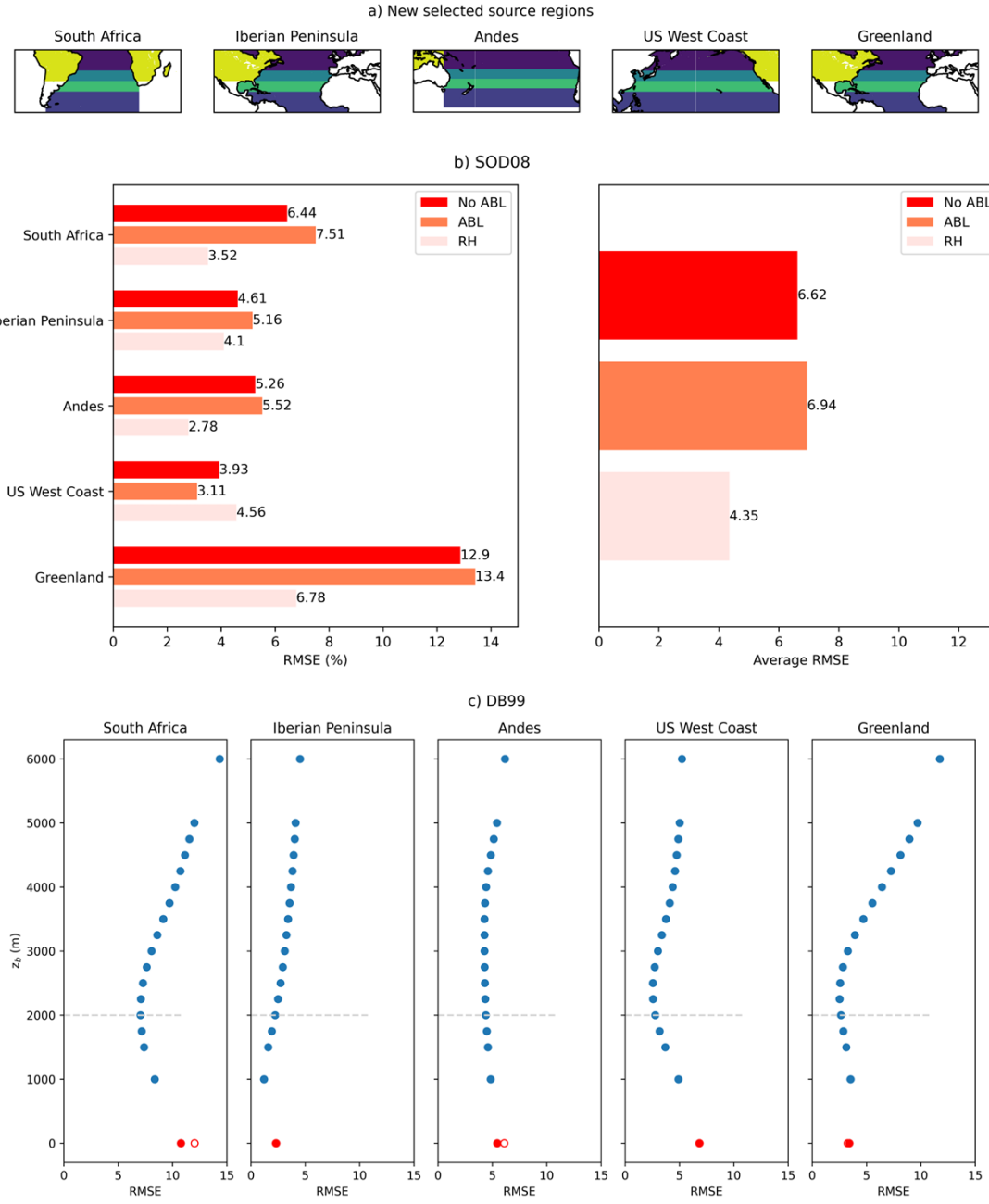

Figure S12: Finer source regions in every oceanic basin containing an AR (panel a) and RMSEs for this new selection of source regions in the case of theSOD08 (panel b) and the DB99 (panel c) diagnostics. The trajectories are generated with FLEXPART-WRF.

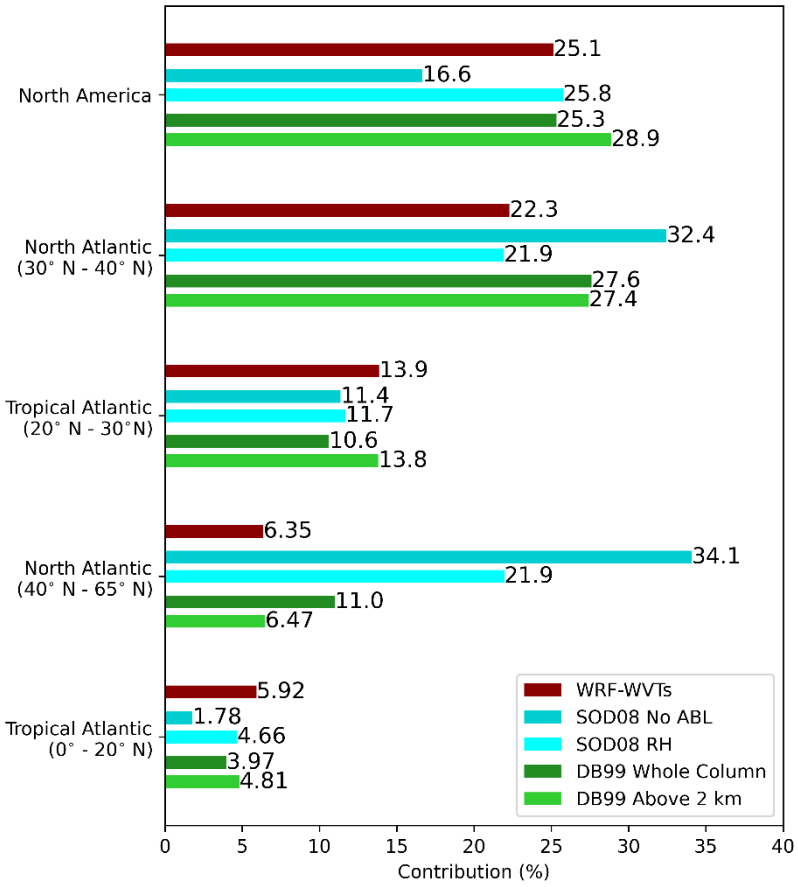

Figure S13: Precipitation fractions computed with WRF-WVTs and the original and modified versions of the SOD08 and DB99 methodologies in the Greenland case. Five source regions are considered, four of them in the North Atlantic Ocean, and the fifth corresponds to North America. Trajectories are generated with FLEXPART-WRF.

	SOD08						DB99			
	RMSE			MAESS			RMSE		MAESS	
	NO ABL	ABL	RH	NO ABL	ABL	RH	Whole Column	Above 2 km	Whole Column	Above 2 km
South Africa	4.83	5.73	2.83	0.73	0.69	0.83	6.26	2.93	0.66	0.83
Iberian Peninsula	3.80	5.01	2.67	0.84	0.79	0.87	2.00	2.08	0.88	0.92
Andes	2.55	1.57	1.73	0.91	0.93	0.93	5.73	4.04	0.81	0.85
US West Coast	2.75	2.67	2.90	0.90	0.90	0.87	5.20	0.66	0.81	0.96
Greenland	12.1	10.3	5.16	0.32	0.24	0.66	3.98	1.79	0.70	0.80
Average	**5.20**	**5.06**	**3.06**	**0.74**	**0.71**	**0.83**	**4.64**	**2.30**	**0.77**	**0.87**

Table S1: RMSE and MAESS for the basic ("No ABL" and "Whole Column") and modified ("RH" and "Above 2 km") configurations for the SOD08 and DB99 methodologies. Results are for trajectories generated with FLEXPART-WRF.

	SOD08						DB99			
	RMSE			MAESS			RMSE		MAESS	
	NO ABL	ABL	RH	NO ABL	ABL	RH	Whole Column	Above 2 km	Whole Column	Above 2 km
South Africa	3.80	5.26	2.65	0.79	0.73	0.83	6.95	1.82	0.62	0.88
Iberian Peninsula	5.77	8.99	2.35	0.77	0.65	0.86	4.38	1.58	0.78	0.90
Andes	3.63	4.60	2.46	0.87	0.84	0.86	8.76	3.31	0.71	0.89
US West Coast	0.84	1.15	1.41	0.96	0.96	0.92	5.07	1.16	0.83	0.95
Greenland	10.9	12.4	4.22	0.47	0.37	0.73	3.42	2.31	0.72	0.76
Average	**4.98**	**6.48**	**2.82**	**0.77**	**0.71**	**0.84**	**5.72**	**2.04**	**0.73**	**0.87**

Table S2: RMSE and MAESS for the basic ("No ABL" and "Whole Column") and modified ("RH" and "Above 2 km") configurations for SOD08 and the DB99 methodologies. Results are for trajectories generated with FLEXPART-ERA5.

References

Brioude, J., Arnold, D., Stohl, A., Cassiani, M., Morton, D., Seibert, P., Angevine, W., Evan, S., Dingwell, A., Fast, J. D., Easter, R. C., Pisso, I., Burkhart, J., and Wotawa, G.: The Lagrangian particle dispersion model FLEXPART-WRF version 3.1, Geosci. Model Dev., 6, 1889–1904, https://doi.org/10.5194/gmd-6-1889-2013, 2013.

Dirmeyer, P. A. and Brubaker, K. L.: Contrasting evaporative moisture sources during the drought of 1988 and the flood of 1993, J. Geophys. Res. Atmospheres, 104, 19383–19397, https://doi.org/10.1029/1999JD900222, 1999.

Insua-Costa, D. and Miguez-Macho, G.: A new moisture tagging capability in the Weather Research and Forecasting model: formulation, validation and application to the 2014 Great Lake-effect snowstorm, Earth Syst. Dyn., 9, 167–185, https://doi.org/10.5194/esd-9-167-2018, 2018.

Pisso, I., Sollum, E., Grythe, H., Kristiansen, N. I., Cassiani, M., Eckhardt, S., Arnold, D., Morton, D., Thompson, R. L., Groot Zwaaftink, C. D., Evangeliou, N., Sodemann, H., Haimberger, L., Henne, S., Brunner, D., Burkhart, J. F., Fouilloux, A., Brioude, J., Philipp, A., Seibert, P., and Stohl, A.: The Lagrangian particle dispersion model FLEXPART version 10.4, Geosci. Model Dev., 12, 4955–4997, https://doi.org/10.5194/gmd-12-4955-2019, 2019.

Tuinenburg, O. A. and Staal, A.: Tracking the global flows of atmospheric moisture and associated uncertainties, Hydrol. Earth Syst. Sci., 24, 2419–2435, https://doi.org/10.5194/hess-24-2419-2020, 2020.